



Study of the threshold anomaly effect in the reaction ${}^7\text{Li}+{}^{208}\text{Pb}$ at energies around the Coulomb barrier

E. Vardaci^{1,2,a}, P. K. Rath^{1,2,3}, M. Mazzocco^{4,5}, A. Di Nitto^{1,2}, G. La Rana^{1,2}, C. Parascandolo^{1,2}, D. Pierroutsakou², M. Romoli², A. Boiano², A. Vanzanella², M. Cinausero⁶, G. Prete⁶, N. Gelli⁷, F. Lucarelli^{7,8}, C. Mazzocchi⁹, M. La Commara^{10,2}, L. Fortunato^{4,5}, A. Guglielmetti^{11,12}, F. Soramel^{4,5}, L. Stroe¹³, C. Signorini⁴

¹ Dipartimento di Fisica “E. Pancini”, Università degli Studi di Napoli “Federico II”, 80126 Naples, Italy

² Istituto Nazionale di Fisica Nucleare, Sezione di Napoli, 80126 Naples, Italy

³ Centurion University of Technology and Management, Gajapati 761211, Odisha, India

⁴ Dipartimento di Fisica e Astronomia “G. Galilei”, Università degli Studi di Padova, 35131 Padua, Italy

⁵ Istituto Nazionale di Fisica Nucleare, Sezione di Padova, 35131 Padua, Italy

⁶ Laboratori Nazionali di Legnaro dell’Istituto Nazionale di Fisica Nucleare, 35020 Padua, Legnaro, Italy

⁷ Istituto Nazionale di Fisica Nucleare, 50019 Florence, Italy

⁸ Dipartimento di Fisica, Università degli Studi di Firenze, 50019 Florence, Italy

⁹ Faculty of Physics, University of Warsaw, PL-02-093 Warsaw, Poland

¹⁰ Dipartimento di Farmacia, Università degli Studi di Napoli “Federico II”, 80126 Naples, Italy

¹¹ Università degli Studi di Milano, dipartimento di fisica, Via celoria 16, 20133 Milano, Italy

¹² Istituto Nazionale di Fisica Nucleare, Sezione di Milano, 20133 Milan, Italy

¹³ Horia Hulubei National Institute for Physics and Nuclear Engineering, Bucharest-Magurele, Romania

Received: 15 January 2021 / Accepted: 12 February 2021 / Published online: 16 March 2021

© The Author(s) 2021

Communicated by Nicolas Alamanos

Abstract The elastic scattering in the reaction ${}^7\text{Li}+{}^{208}\text{Pb}$ was investigated in the bombarding energy range from 25 to 39 MeV. The real and imaginary parts of the optical potential were analyzed by using a phenomenological potential. A dispersion relation analysis is presented in order to investigate the threshold anomaly effect. It is concluded that ${}^7\text{Li}$ has an intermediate behavior between the tightly bound nuclei such as ${}^{16}\text{O}$ and the loosely bound nuclei such as ${}^6\text{Li}$ where the lack of the threshold anomaly is unambiguously observed. Reaction cross sections are also extracted from the elastic scattering data and its comparison with the ones of other systems has been performed to draw hints on the effect of the breakup channel.

1 Introduction

The study of elastic scattering around the Coulomb barrier is the simplest mean to determine the energy dependence of the real and imaginary parts of the optical potential (OP) in a nuclear reaction.

In reactions between stable heavy ions, it was shown [1–3] that the so-called threshold anomaly (TA) effect occurs. This

effect concerns with the observation of a localized peak in the real part of the OP accompanying a sharp decrease of the imaginary part as the bombarding energy declines toward the Coulomb barrier. At higher energies, both the real and imaginary potentials are almost energy independent.

It was shown [2,4] that such a suspected anomaly, which is interpreted as a possible consequence of a strong coupling between the elastic scattering channel to other reaction channels, is quite a general property of heavy ion optical potentials at energies approaching the Coulomb barrier, where the flux into non-elastic channels is drastically hindered. The behavior of the real and imaginary parts of the OP is indeed the consequence of the causality principle [4] which states that a scattered wave cannot be emitted before the arrival of the incident wave. This principle implies the existence of a dispersion relation which connects the energy variation of the real potential to that of the imaginary potential through a principal part integral. Such a connection gives rise to the localized peak in the real part of the OP [4] and the sudden drop in the imaginary part.

This picture may change when loosely bound (stable or radioactive) nuclei are involved in the scattering process [5]. These nuclei have binding energies of few MeV and hence, they are characterized by a larger breakup (BU) and cluster transfer probability. If one of the colliding partner is a

^a e-mail: vardaci@na.infn.it (corresponding author)

weakly bound nucleus, and even more especially a low- Z nucleus, breakup may occur at energies below the Coulomb barrier (it is not suppressed around and below the barrier energies). Consequently, (1) the imaginary part of the OP may not decrease as sharply as in the case of tightly bound nuclei since it must take into account the non negligible breakup and transfer cross-sections at energies below the barrier, and (2) the real part of the OP may not show the typical barrier in consequence of the dispersion relation. In such a condition, the usual TA may not be observed, hence, the new anomaly could be the absence of the TA. This situation has been named breakup threshold anomaly (BTA) [6], namely, BTA is the absence of TA at the Coulomb barrier.

Concerning this issue, many conflicting experimental results have been reported when using stable loosely bound nuclei, especially when considering ${}^6\text{Li}$ or ${}^7\text{Li}$ as projectiles. The BTA has been investigated in a large number of nuclear systems involving loosely bound projectiles with a variety of medium and large mass targets, for instance ${}^9\text{Be}$ on ${}^{27}\text{Al}$ [7], ${}^{64}\text{Zn}$ [8–11], ${}^{144}\text{Sm}$ [12, 13], ${}^{208}\text{Pb}$ and ${}^{209}\text{Bi}$ [14, 15]; ${}^6\text{Li}$ and ${}^7\text{Li}$ on ${}^{208}\text{Pb}$ [6, 16–22], on ${}^{27}\text{Al}$ [23–25], ${}^{144}\text{Sm}$ [26], ${}^{58,64}\text{Ni}$ [27, 28], ${}^{59}\text{Co}$ [29], ${}^{90}\text{Zr}$ [30], ${}^{138}\text{Ba}$ [9, 31, 32] and ${}^{28}\text{Si}$ [20].

When light weakly bound radioactive projectiles are involved, the general framework of the occurrence or not of the BTA is still far from being clarified. Existing measurements concern with the neutron-rich nucleus ${}^6\text{He}$ [33–35], the proton-rich nuclei ${}^8\text{B}$ [36–39] and ${}^7\text{Be}$ [40–42] on various targets. However, the complexity of such studies, due to a large extent to the limited beam intensity and purity, affects the major conclusions and further investigations are mandatory.

For what it concerns stable loosely bound nuclei, the most striking case is the one of reactions involving ${}^6\text{Li}$ and ${}^7\text{Li}$ as projectiles. Although the BTA was observed in all systems involving ${}^6\text{Li}$, for ${}^7\text{Li}$ its presence is observed in some systems. In the case of ${}^6\text{Li}$ on various targets, such as ${}^{27}\text{Al}$ [23], ${}^{64}\text{Ni}$ [27], ${}^{64}\text{Zn}$ [11], ${}^{80}\text{Se}$ [43], ${}^{90}\text{Zr}$ [30], ${}^{116,112}\text{Sn}$ [44], ${}^{138}\text{Ba}$ [31], ${}^{144}\text{Sm}$ [26], ${}^{208}\text{Pb}$ [16], ${}^{209}\text{Bi}$ [45] and ${}^{232}\text{Th}$ [46], a small increase in the imaginary part of the optical potential, rather than a decrease to zero, at energies below the Coulomb barrier was observed. This indicates the absence of the usual TA. In the cases of elastic scattering induced by ${}^7\text{Li}$ on ${}^{59}\text{Co}$ [29], ${}^{80}\text{Se}$ [43], ${}^{138}\text{Ba}$ [31], and ${}^{208}\text{Pb}$ [16], however, only the conventional TA was identified, even though ${}^7\text{Li}$ is considered as a loosely bound nucleus. Contradictory results have also been reported for ${}^{138}\text{Ba}$ [9] and ${}^{28}\text{Si}$ [20, 47] targets, where the BTA has been observed for both ${}^6\text{Li}$ and ${}^7\text{Li}$ projectiles. In short, the BTA has been observed using ${}^6\text{Li}$ as a projectile but controversial results are reported for ${}^7\text{Li}$. In addition, there are only few measurements using ${}^7\text{Li}$ as projectile compared to ${}^6\text{Li}$.

In the present work we show the results of our investigation of the elastic scattering of the system ${}^7\text{Li} + {}^{208}\text{Pb}$ at bombarding energies ranging from below (even lower than the one reported in [16]) to above the Coulomb barrier ($V_C \sim 30$ MeV in the c.m. and $V_C \sim 31$ MeV in the lab frame). ${}^7\text{Li}$ is a weakly bound nucleus and has a breakup threshold energy (in $\alpha+t$) of 2.47 MeV, just 1 MeV above the breakup threshold of ${}^6\text{Li}$ (in $\alpha+d$, 1.48 MeV). In the case of ${}^6\text{Li}$, there are no unbound excited states below the breakup threshold, whereas ${}^7\text{Li}$ has one bound excited state below 2.47 MeV at $E^* = 0.478$ MeV. The effect that the dicluster structure of ${}^7\text{Li}$ has on the breakup and other processes, such as electromagnetic excitation and radiative capture, has been theoretically investigated in [48, 49]. Hence, it is interesting to explore how the breakup of ${}^7\text{Li}$ will affect the elastic scattering compared to ${}^6\text{Li}$ case which has a larger breakup probability. Indeed, the experiment was designed to measure the inclusive and exclusive breakup cross sections (in $\alpha+p,d,t$) of the projectile ${}^7\text{Li}$ with a 4π light charged particle detector. In this article we report only on the elastic scattering channel.

It is important to note that the elastic channel of the system ${}^7\text{Li} + {}^{208}\text{Pb}$ was already investigated in the works in Refs. [16–18, 22], at energies around the barrier, and contradictory results have emerged. In the works in Refs. [16–18], in which the elastic scattering was measured with a high angular resolution, it was concluded, on the basis of a detailed optical model analysis, that ${}^7\text{Li}$ shows evidence of the usual TA only. In the more recent work by Zerva et al. [22] a different result is achieved. By using the quasi-elastic backscattering approach, it was found out that ${}^7\text{Li}$ shows an intermediate behavior, namely, the imaginary potential drops properly as in the case of well bound nuclei but the real potential shows not connection with the dispersion relation.

Here, we report on the extension of the data set on the system ${}^7\text{Li} + {}^{208}\text{Pb}$ to a subbarrier energy up to 25 MeV with the aim to increase sensibly the event statistics by taking advantage of the 4π angular coverage of the detector array $8\pi\text{LP}$. Elastic scattering angular distributions were measured at bombarding energy from 25 to 39 MeV. In the data analysis shown further we will analyze the impact of this additional point at 25 MeV on the trend of the real and imaginary potential.

The experimental angular distributions of the elastic channel are analyzed within the framework of the optical model as implemented in the code FRESKO [50]. This code was also used to extract the excitation function of the reaction cross section. The study presented here is the natural continuation of the ones initiated on ${}^6\text{Li} + {}^{208}\text{Pb}$, carried out with the same experimental setup [51–54] and reveals a new aspect of ${}^7\text{Li}$.

The article is divided in the following sections: Sect. 2 contains experimental details and data analysis. The optical model analysis of elastic scattering and of the threshold anomaly is presented in Sect. 3. The reaction cross section

is analyzed in Sect. 4. Finally, we present the summary and conclusions in Sect. 5.

2 Experimental details and data analysis

The experiment was performed using a pulsed beam of ${}^7\text{Li}^{3+}$ delivered by XTU-Tandem accelerator at Laboratori Nazionali di Legnaro (LNL, Italy). The reaction ${}^7\text{Li} + {}^{208}\text{Pb}$ was run at the beam energies of 25, 31, 33, 35, and 39 MeV covering the range from below to above the Coulomb barrier $V_C = 30.1$ MeV corresponding to $E_{c.m.}/V_C = 0.80, 1, 1.06, 1.12, 1.25$. $E_{c.m.}$ is the energy available in the center of mass frame. The pulsed beam had a period of 800 ns and duration of around 2 ns. An enriched self-supporting $200 \mu\text{g}/\text{cm}^2$ thick ${}^{208}\text{Pb}$ target was used.

The elastically scattered ${}^7\text{Li}$ ions were detected with the 4π array $8\pi\text{LP}$ described in detail in [55,56]. The array $8\pi\text{LP}$, shown schematically in Fig. 1, is made of two main sectors: a Wall, covering the angles from 2.5° to 24° and the Ball, covering the angles from 34° up to 163° .

The Ball is a sphere of 126 (ΔE -E) telescopes which are arranged in 7 rings labeled from A to G and placed co-axially around the beam axis. Each telescope consists of a ΔE silicon detector ($300 \mu\text{m}$ thick), backed by a CsI scintillator (5 mm thick). Each ring contains 18 identical telescopes and covers about 17° in the polar angle and from 0° to 360° in the azimuthal angle. For this experiment, inside the Ball sector, we have installed a cylinder placed co-axially around the beam to reduce the opening of the active area of the Ball telescopes, the count rate and the dead time. In this way, the measurements were taken at the laboratory angles shown in Table 1. The data in Table 1 come from a Monte Carlo simulation of the geometry of $8\pi\text{LP}$ and are consistent with the

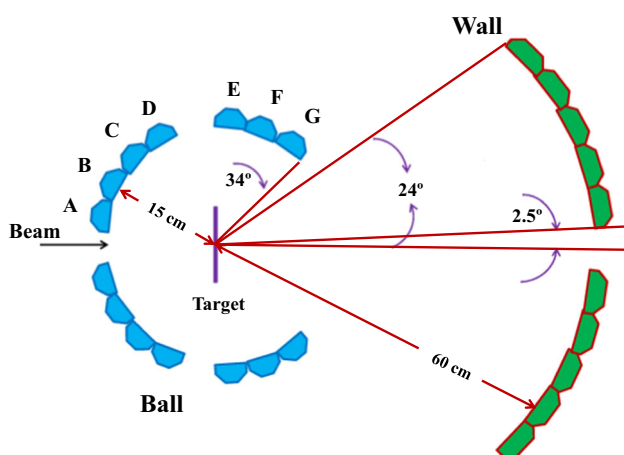


Fig. 1 Schematic layout of the experimental apparatus $8\pi\text{LP}$. The letters from A to G label the seven rings of the Ball section

Table 1 Laboratory angle of each Ball ring at which the angular distributions were measured and associated angular opening

Ring	Θ_{lab} ($^\circ$)	Angular opening ($^\circ$)	Solid angle (msr)
A	156.5	± 1.7	2.88
B	137.7	± 1.9	3.40
C	119.5	± 1.9	3.35
D	103.3	± 1.8	3.22
E	76.7	± 1.8	3.21
F	60.5	± 1.9	3.42
G	48.9	± 0.8	0.68

measurements obtained from the mechanical design of the inner cylinder.

The Wall is a matrix of 11×11 ΔE -E telescopes. The only ones missing are the four at the corners and the central one to allow the exit of the beam. Each telescope has an active area of 25 cm^2 , an angular coverage of 4° , and subtends a solid angle of about 7 msr. Each telescope is independently fixed to an aluminum support structure. All the detectors in the Wall are in close contact between each other to form a portion of spherical surface with a radius of 60 cm. Also for the Wall sector, we have used for this experiment a thick aluminum screen to reduce the active area of the telescopes, and therefore the solid angle. In this case the angular opening of each telescope is about one degree.

Each telescope of the Wall and Ball embeds also the preamplifiers for the ΔE and E sectors. A cooling system, based on a circulating refrigerant liquid, keeps the whole system at a stable temperature. The cooling system is crucial to guarantee the stability of the performance of the whole detector system.

Particle identification is carried out by using the ΔE -E technique for particles that have energy enough to pass through the ΔE stage. For particles that stop in the ΔE stage two different methods are used. For the Ball telescopes, the Pulse Shape Discrimination technique is used being the Si stage mounted in the flipped configuration. For the Wall telescopes, the Time-of-Flight (TOF) technique is used. The reference time is taken from the radio frequency signal of the pulsed beam. This system allows a very good identification of light charged particles, namely, α particles, tritons, deuterons and protons. ${}^7\text{Li}$ was completely stopped in the ΔE in the studied energy range. Figure 2a shows a sample of a Time vs. ΔE matrix, whereas Fig. 2b shows the ΔE vs. ER (residual energy) matrix from the same detector for the 33 MeV ${}^7\text{Li}$ beam. One can observe the high quality of the separation between protons, deuterons, tritons and α particles in both matrices.

The acquisition system is based on the FAIR (FAst Inter-crate Readout) [57] and VIPERS (Vme Interfaced to Pci Easy

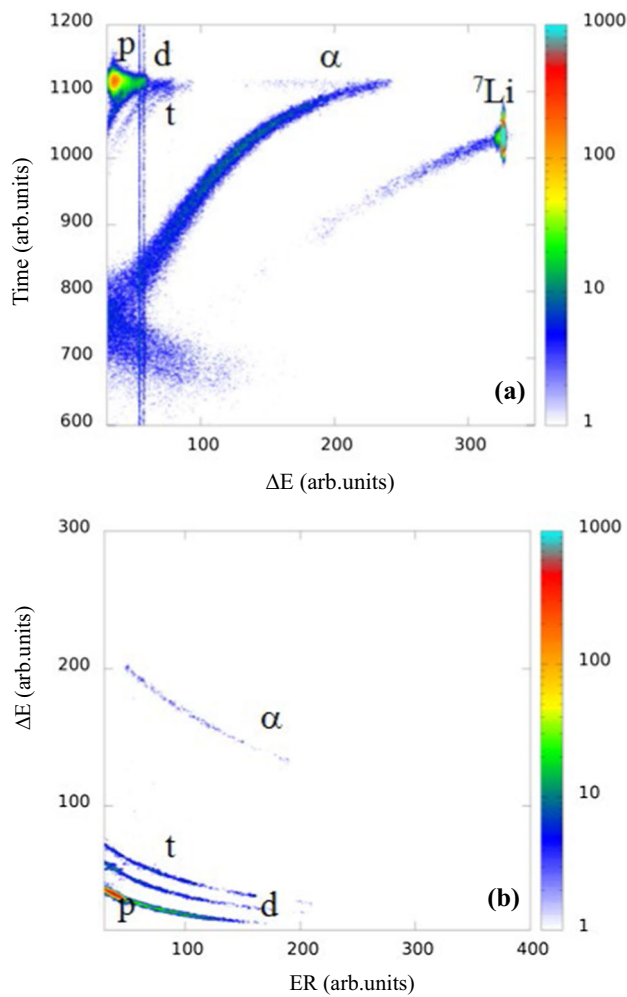


Fig. 2 Experimental matrices from a Ball telescope at lab forward angle ($\theta=43^\circ$ and $\phi=320^\circ$). **a** Time vs. ΔE matrix for the particles that stop in the ΔE stage; **b** same telescope but in residual energy ΔE vs. ER (residual energy) matrix for the particles that stop in the E stage. Protons, deuterons, tritons and α particle energy spectra are obtained by summing the energy ER + ΔE

Readout System) [58–63] systems running a VME (Versa Module Europa) front-end with commercial TDC (Time-to-Digital Converter) and ADC (Analog-to-Digital Converter) modules. The trigger was arranged to register single and coincidence events between telescopes. The coincidence trigger was implemented to detect light charged particles (protons, deuterons, tritons and α particles) in coincidence to study breakup channels.

The experimental elastic scattering angular distributions, normalized to the Rutherford differential cross section, are shown in Fig. 3 for all laboratory energies. The angular distributions in linear scale are shown in Fig. 4. The experimental errors in the center of mass angle θ_{cm} are within the size of the symbols. The large statistics at angles $\theta_{c.m.} > 40^\circ$ could be reached, especially at the sub-barrier energy, because of the 360° azimuthal coverage of the 8π LP array and the notewor-

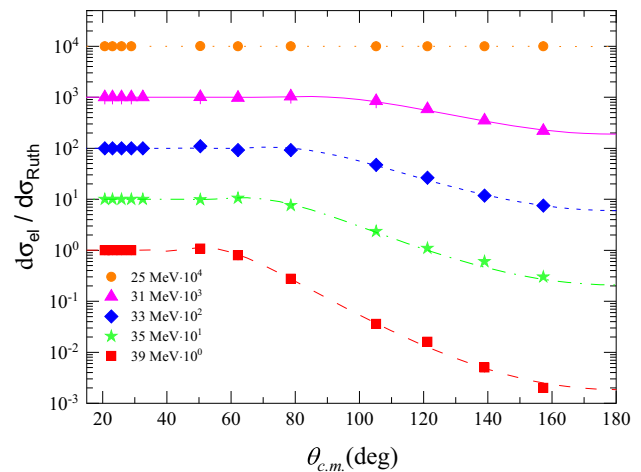


Fig. 3 Elastic scattering angular distributions of the system ${}^7\text{Li}+{}^{208}\text{Pb}$ at various bombarding energies normalized to the respective Rutherford differential cross section vs. the c.m. angle $\theta_{c.m.}$. The points are the experimental data. The solid lines represent the best fit of the optical model computed with a phenomenological potential and the code FRESKO

thy stability of the XTU-Tandem Accelerator at LNL. The number of events at a given laboratory angle with respect to the beam, each corresponding to a specific ring of the Ball (Fig. 1), is obtained by adding the yields of 18 detectors in the same ring. This is possible because of the spherical symmetry of the Ball. This symmetry of the 8π LP setup turns out to be a crucial advantage when various reaction channels, especially those of relatively smaller cross section, are studied in the same experiment [64–67].

We mark that the angular distributions from 31 up to 39 MeV well match the data from Martel et al. [18]. This result gives us confidence on the normalization and angular resolution of our new data measured at 25 MeV.

An additional feature of the 8π LP detector is the stability of the energy resolution of the ΔE stages. In Fig. 5 we show the energy spectrum of the elastic scattered ${}^7\text{Li}$ detected at 156° in the lab frame in the reaction at the bombarding energy of 25 MeV. On the left of the main peak corresponding to the ground state, there is also the tiny peak corresponding to the first excited level of ${}^7\text{Li}$, only about half an MeV apart.

3 Optical model analysis of elastic scattering

In order to proceed to the analysis of the threshold anomaly, it is necessary to perform the analysis of the elastic scattering data with the optical model. This task will be developed in the first subsection. In the second subsection we will proceed to the dispersion analysis.

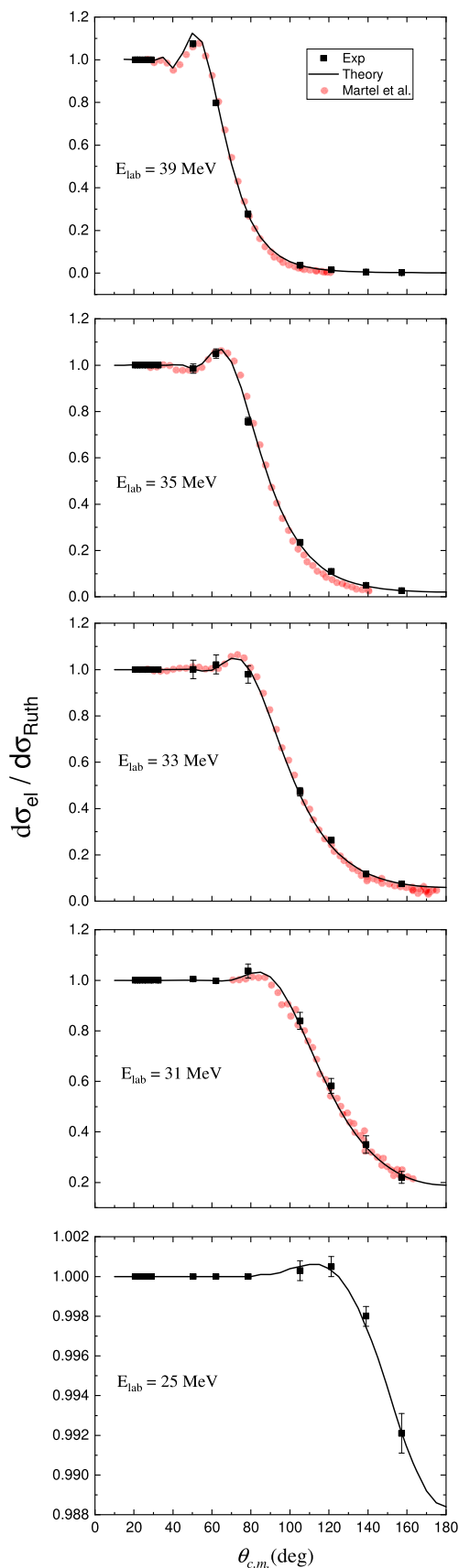


Fig. 4 Same as in Fig. 3 but in linear scale. The square symbols are big enough to include the uncertainty of the angle. The error in the cross section ratio is visible if bigger than the symbol. Data extracted from Fig. 1 in Martel et al. [18] are shown as red bullets

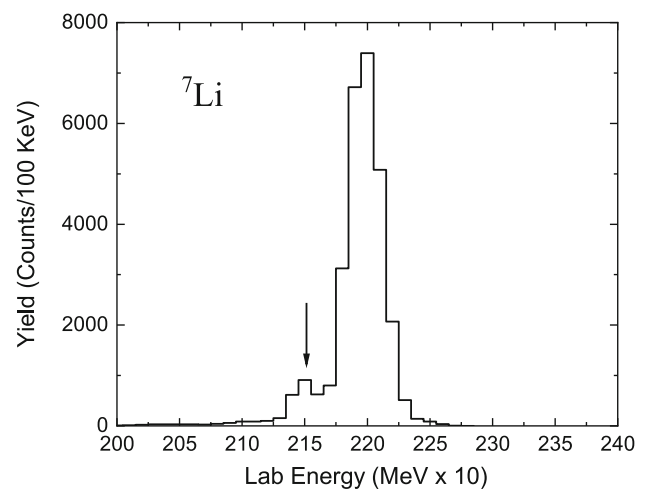


Fig. 5 Energy spectrum of elastic scattered ${}^7\text{Li}$ ions at 156° in the lab frame. The bombarding energy is 25 MeV. The arrow indicates the energy corresponding the first excited level at 0.477 MeV

3.1 Phenomenological analysis with Woods-Saxon potential

The analysis of the elastic scattering angular distribution was performed using the optical model (OM) in which the diffusion process between two particles is reduced to the motion of a point particle in a local and complex effective potential. The effective uni-dimensional potential $U(r)$ is a function of the distance r between the two particles. To describe the removal of particles from the elastic channel, the potential is built as the sum of a real $V(r)$ and imaginary component $W(r)$ as:

$$U(r) = V(r) + i W(r) \tag{1}$$

The potential is considered to be independent from the energy of the colliding particles, but as it will be shown, such dependence is indeed an important ingredient that raises when the relative energy reaches the vicinity of the Coulomb barrier [4]. The functions representing $V(r)$ and $W(r)$ are chosen on an empirical basis. The widely used choice is the Woods-Saxon type

$$U(r) = V_C(r) - V_0 f(r; R_V, a_V) - i W_0 f(r; R_W, a_W) \tag{2}$$

where

$$f(r; R_i, a_i) = \left[1 + \exp\left(\frac{r - R_i}{a_i}\right) \right]^{-1} \tag{3}$$

$$R_i = r_i \left(A_P^{1/3} + A_T^{1/3} \right) \quad i = V, W \tag{4}$$

V_0 and W_0 are the real and imaginary potential strengths, and r_i and a_i the reduced radii and diffuseness, respectively.

Table 2 Best fit parameters of the phenomenological optical potential for the reaction ${}^7\text{Li}+{}^{208}\text{Pb}$. The reaction cross sections σ_R were estimated from FRESKO code calculations after fitting the elastic scattering angular distribution shown in Fig.3

E_{lab} (MeV)	V_0 (MeV)	$a_V = a_W$ (fm)	W_0 (MeV)	$r_V = r_W$ (fm)	χ^2	σ_R (mb)
25.0	62.00	0.52	10.32	1.27	1.03	1.18
31.0	60.00	0.52	32.00	1.27	0.26	317
33.0	60.84	0.52	45.00	1.27	0.23	584
35.0	58.84	0.52	46.70	1.27	0.18	811
39.0	77.81	0.52	44.70	1.27	1.04	1240

$f(r; R_i, a_i)$ is the form factor of the Woods-Saxon potential. A_P and A_T are the projectile and target mass numbers, respectively. $V_C(r)$ is the Coulomb potential between two charged spheres representing the projectile and target nuclei.

The six adjustable parameters, V_0 , r_V , a_V , W_0 , r_W and a_W are fixed by fitting the elastic scattering angular distributions at each bombarding energy. However, it is well known that more than one set of these free parameters can provide equally good fit to the elastic scattering angular distributions. This ambiguity in the determination of the parameters' values, firstly noted by Igo [68], has been largely investigated in the literature and manifests the fact that the number of parameters is redundant. It is in fact very commonly found that the change of the potential in the interior of the nucleus (corresponding to large overlap), as a consequence of the choice of different set of free parameters, does not have any influence on the fit to the elastic angular distribution. In particular, only the magnitude of both real and imaginary potential in the surface region is important. In other words, the elastic scattering is principally determined by the value of the OP near some interaction radius. This is quite reasonable from the physical point of view because using only the elastic scattering data the OM can probe only to what extent the elastic scattering is removed from the flux and does not offers constrains, from the elastic data alone, on the potential and wave functions inside the nucleus.

The ambiguity in the values of the free parameters is therefore a direct consequence of the fact that elastic scattering data can only probe the scattering process at the surface of the two colliding nuclei. This widely recognized result has given rise to the concept of the *sensitivity radius* R_S , the radial distance at which the real and imaginary potentials, obtained with multiple sets of parameters that fit the elastic data, cross each other, respectively. To reach out the potential inside the nucleus, inelastic channels must be studied. In this section we will estimate the sensitivity radius R_S for the present data.

In analyzing our data, we had to deal with the same problem of parameters redundancy. We used a grid of values for

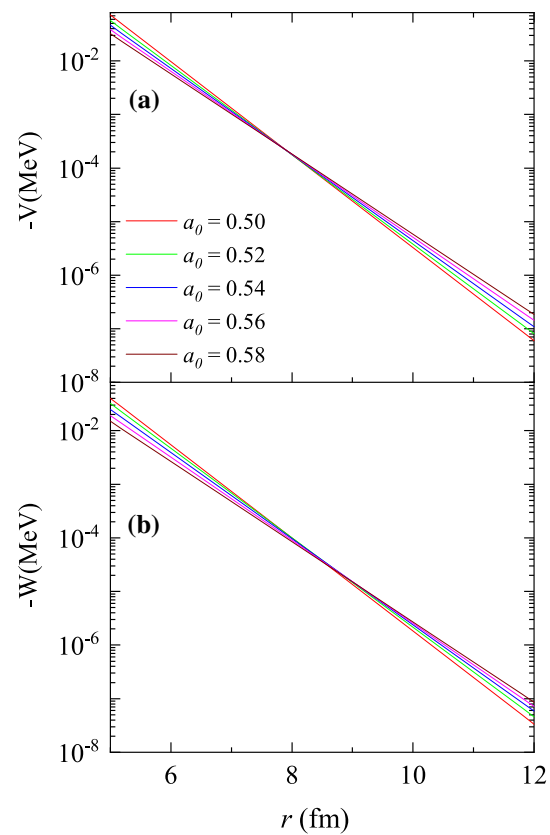


Fig. 6 Real (a) and imaginary (b) potentials that provide similar fits of the data for elastic scattering at 39 MeV. Reduced radii and diffuseness are the same for both potentials. The crossing points define the real (a) and imaginary (b) sensitivity radii, respectively

the six parameters to fit the angular distributions at all measured energies. Very good fits to the data were obtained with minimum χ^2 but, as expected, we found several families of optical potential parameters that could describe the angular distributions equally well. We soon realized that we could obtain equally good fit by imposing the constraints:

$$R_0 = R_V = R_W \quad a_0 = a_V = a_W. \quad (5)$$

In this way the above redundancy is excluded by reducing the number of parameters to four without affecting the quality of the goodness of the fit. The best fit parameters are shown in Table 2 and the obtained angular distributions are shown as solid lines in Figs. 3 and 4.

By spanning the family of potentials that would fit the data, we could also estimate the sensitivity radius. Figure 6 shows the families of potentials that provide similar fits to the data at 39 MeV. Similar plots were obtained for the other bombarding energies. A diffuseness ranging from $a_0 = 0.50$ fm up to 0.91 fm would produce equally good fit to the experimental angular distributions at all energies. Also for the present reactions, we observe the crossing of the potentials in a narrow

radial distance. In particular, the sensitivity radii $R_{SV} = 7.9$ fm and $R_{SW} = 8.6$ fm corresponding to the real and imaginary radii were obtained. Taking the average of the two, as a general practice, does not change the quality of the fit. Therefore, throughout the following calculations we used the sensitivity radius $R_S = 8.2 \pm 0.4$ fm for the real and imaginary potential.

It is quite evident that the parameters of the potentials, in particular the strength, depend on the bombarding energy. This is another important weakness of the OM because, in principle, the potentials should not depend on the energy and, besides few cases, there is no need to introduce such dependence to reproduce elastic scattering data [4]. Inside the variations of the parameters' values the dynamics of the entrance channel is indeed embedded as well as the competition with other reactions channels, such as inelastic channels, an important consequence of which is the threshold anomaly that will be analyzed in the next subsection.

Since the elastic scattering data are only sensitive to the potential at the sensitivity radius R_S , it is worth to analyze the dependence of the OP, computed at this radius, as a function of the energy. We show in Fig. 7 the values of the real and imaginary potentials, computed at the radius R_S , as a function of the bombarding energy. The error bars come from the uncertainty of the sensitivity radius and of the fitted parameters. It is fairly evident that for energies above the barrier both potentials tend toward a constant value. However, a sudden drop of the imaginary potential appears when approaching the Coulomb barrier V_C , accompanied by the raise of the real one. Both potentials finally drop at sub-barrier energies. This correlated behavior of both potentials is the object of the so-called ‘‘threshold anomaly’’

3.2 Dispersion relation analysis

According to Mahaux et al. [4], the correlated behavior of the real and imaginary potential around the barrier is the consequence of the causality principle that states that a scattered wave cannot be emitted before the interaction has occurred. The application of this principle gives rise to a dispersion relation.

If the real part of the OP is written in this form:

$$V(r, E) = V_0(r) + \Delta V(r, E) \tag{6}$$

then the dispersion relation is [4]:

$$\Delta V(r, E) = \frac{1}{\pi} \mathbf{P} \int_0^\infty \frac{W(r, E')}{E - E'} dE' \tag{7}$$

where \mathbf{P} denotes the principal value. The OP, with the explicit energy dependence, is now written as:

$$U(r, E) = V(r, E) + iW(r, E) \tag{8}$$

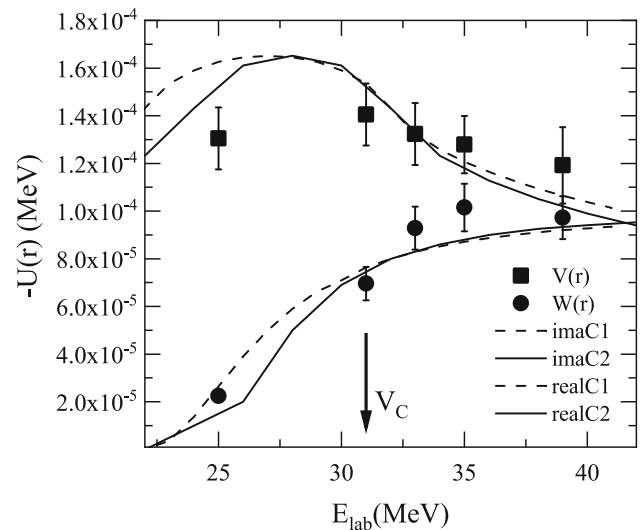


Fig. 7 Energy dependence of the real and imaginary potentials at $R_S = 8.2$ fm for the system ${}^7\text{Li}+{}^{208}\text{Pb}$. The points are the values of the real and the imaginary potentials computed at the sensitivity radius from the optical potential analysis. For the imaginary potential $W(R_S, E_{lab})$, the dashed (imaC1) and solid (imaC2) lines represent two linear-segments approximations; the corresponding curves for the real potential $V(R_S, E_{lab})$ (realC1 and realC2, respectively) were computed from Eqs. 6 and 7. The arrow indicates the laboratory frame Coulomb barrier $V_C = 31.1$ MeV

One consequence of Eq. 7 is that the real potential must be a function of the energy. In particular, any rapid local variation of the imaginary potential $W(r, E)$ is accompanied by a similarly rapid local variation of $V(r, E)$. In particular, if $|W|$ (where $W < 0$) increases rapidly over some small energy range (as in Fig. 7), the associated contribution to ΔV will be attractive ($\Delta V < 0$) in that same energy range. Since it is expected that the function W will always rapidly increase when non-elastic channels open (a threshold behavior), the effect on the real potential V (initially unexpected and so-called an ‘‘anomaly’’) should be a universal phenomenon [4]. In other words, the dispersion relation ensures that the apparent anomalous behavior of the real potential is associated with the closing of non-elastic channels. Consequently, a smoother behavior of the imaginary potential would imply the opening of non-elastic channels, the so called BTA, when the Coulomb barrier is spanned.

As stated in the introduction, the TA is expected to disappear when the breakup channels become important [6] as in the case of the weakly bound nuclei, such as ${}^6\text{Li}$. The lack of a TA has been termed as BTA [6]. To analyze the occurrence or not of a TA in our system ${}^7\text{Li}+{}^{208}\text{Pb}$, we have carried out the analysis of the dispersion relation at the energies around the Coulomb barrier. To evaluate the integral in Eq. 7, at the sensitivity radius, we need a functional form which describes the imaginary potential in Fig. 7. As proposed in [4], we used an empirical linear-segment approximation. In particular, we

show two approximations in Fig. 7 for the imaginary potential to investigate the effect of the choice of a linear-segment approximation on the real potential. By using Eqs. 6 and 7 we computed the real potential curves shown in Fig. 7. We observe that the real part of the potential remains nearly constant at higher energies ($E \geq V_C$), whereas it shows a nearly bell shape in the energy region of the barrier where the imaginary potential drops. Going toward lower energies, when the imaginary potential W starts decreasing below the barrier, the real potential V does show an increasing trend quite well reproduced by the dispersion relation calculation.

At energies far below the barrier, the further drop of the imaginary potential produces the lowering of the real potential, but not enough to fit into the experimental point of V at 25 MeV. To reproduce it, we should force the empirical imaginary potential to drop even more rapidly than the solid line in Fig. 7. However, in this way, the point of W at 25 MeV would not be intercepted. As a general trend, we can conclude that even if we change slightly the slope of the empirical imaginary potential, the bell shape of the real potential persists. In particular, the smoother is the drop in W the broader is the bell shaped curve in V .

From this analysis, it appears that in the reaction with the weakly bound ${}^7\text{Li}$, contrarily to what is regularly found with ${}^6\text{Li}$, the TA does occur but it is not as sharply identified as in other typical reactions with tightly bound projectiles. The experimental point at 25 MeV marks this difference. The artificial faster drop in W necessary to reproduce the real potential at 25 MeV is not compatible with the measured imaginary potential at the same energy. Therefore, it seems that ${}^7\text{Li}$ bridges the case of clear BTA occurring in ${}^6\text{Li}$ and the case of sharp TA occurring in tightly bound nuclei. These findings may provide a key to explain the controversial results found in the literature for ${}^7\text{Li}$, where a point at such low energy of 25 MeV has never been measured before.

One possible explanation of this intermediate behavior of ${}^7\text{Li}$ could be the occurrence at barrier of single-nucleon transfer channels. Indications on this regards were explored in the work by Keeley and Rusek [69] where the coupling with the transfer channel ${}^{208}\text{Pb}({}^7\text{Li}, {}^6\text{Li}){}^{209}\text{Pb}$ was studied. The present result offers a further constraint to refine such optical model calculations with coupling to transfer channels at the barrier.

4 Reaction cross-section

The reaction cross sections σ_R , as function of the bombarding energy, for the system ${}^7\text{Li}+{}^{208}\text{Pb}$, were evaluated from the measured elastic scattering angular distributions using the code FRESKO and is shown in the last column of Table 2. In Fig. 8a σ_R is compared with literature data on the systems ${}^{6,7,8}\text{Li}+{}^{208}\text{Pb}$ [70]. The figure shows an excellent agreement

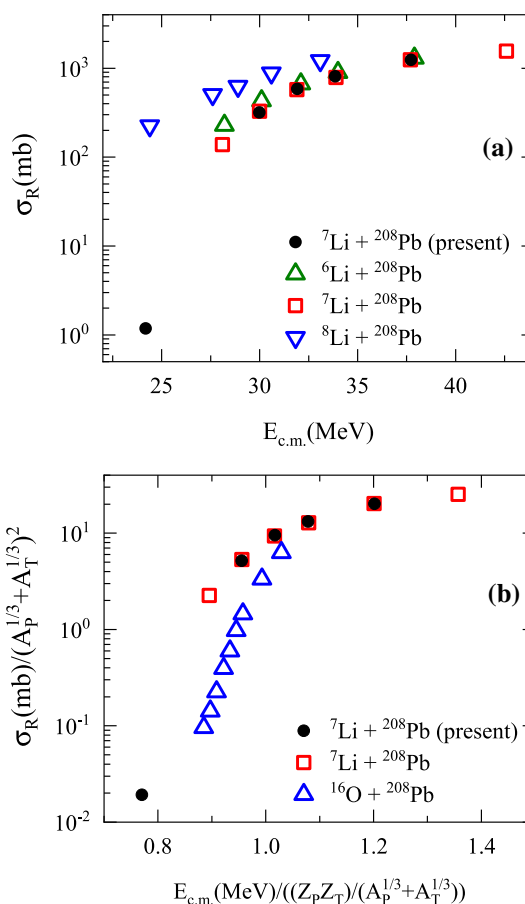


Fig. 8 **a** Reaction cross sections vs. center of mass energy for the systems ${}^{6,7,8}\text{Li}+{}^{208}\text{Pb}$ (${}^6\text{Li}+{}^{208}\text{Pb}$ (Δ) from [70], ${}^7\text{Li}+{}^{208}\text{Pb}$ (\bullet) present work and (\square) from [70], ${}^8\text{Li}+{}^{208}\text{Pb}$ (∇) from [71]). **b** Reduced reaction cross section and projectile energy (following the prescription given in [8]) for the systems ${}^7\text{Li}+{}^{208}\text{Pb}$ (present data (\bullet) and in [70] (\square)) and ${}^{16}\text{O}+{}^{208}\text{Pb}$ [72] (Δ)

with other measurements and the impact of the point at 25 MeV.

In Fig. 8b reaction cross sections of two systems are compared by using the reduced variables prescription suggested by Gomes et al. [8] when comparing cross sections between different systems. The reduction method aims at eliminating the dependence of the reaction cross section on geometrical and barrier dependent terms. For this reason, the reaction cross section is normalized to $(A_P^{1/3} + A_T^{1/3})^2$ and the center of mass energy is divided by the Coulomb barrier term $Z_P Z_T / (A_P^{1/3} + A_T^{1/3})$. The indexes P and T refer to the projectile and target nuclei, respectively. The comparison, in this reduced scale, with the strongly bound projectile in the system ${}^{16}\text{O}+{}^{208}\text{Pb}$ clearly shows that the reaction cross section is larger for the weakly bound ${}^7\text{Li}$ projectile going toward the region of decreasing energy. This is quite a common result [8,44] when reaction cross sections in reactions induced by tightly and loosely bound nuclei are compared,

as in the case of Fig. 8b. To explain this finding it is quite common to resort to the expectation that loosely bound nuclei have a larger breakup probability at energies around the barriers. This will open up channels not accessible to tightly bound nuclei because of their larger binding energy, with a consequential larger reaction cross section. Our reaction cross section data for the system ${}^7\text{Li}+{}^{208}\text{Pb}$ confirm this trend, which is even more strengthened at the deep sub-barrier energy measured.

5 Conclusion and summary

Elastic scattering angular distributions were measured for the system ${}^7\text{Li}+{}^{208}\text{Pb}$ at the laboratory energy of 25, 31, 33, 35 and 39 MeV (0.80–1.25 times the Coulomb barrier). The experimental data were analyzed by using phenomenological optical potentials. The behavior of the real and imaginary part of the potential as a function of bombarding energy is consistent with a situation which is intermediate between the presence of a threshold anomaly and the well assessed breakup threshold anomaly found in ${}^6\text{Li}$ induced reactions. This conclusion is in substantial agreement with the result of Ref. [22] and in disagreement with Refs. [16–18]. This means that the controversial behavior of ${}^7\text{Li}$ needs further investigation, for instance, of the inelastic channel and of possible transfer channels opening at the Coulomb barrier not accounted for in the optical model calculations. The analysis of the breakup channels undertaken with this experiment will certainly provide further elements on these regards.

The reaction cross section has been extracted and compared with the ones of other systems. It turns out that ${}^7\text{Li}$ behaves more like a loosely bound nucleus than a tightly bound one. This intermediate behavior ${}^7\text{Li}$ around the Coulomb barrier confirms the necessity of additional studies.

Acknowledgements We are very much thankful to the operating staff of the Laboratory Nazionali di Legnaro for the smooth running of the accelerator during the experiment. One of us (PKR) acknowledges the financial support from the Department of Physics at University of Naples and INFN, Sezione di Napoli.

Funding Open access funding provided by Università degli Studi di Napoli Federico II within the CRUI-CARE Agreement.

Data Availability Statement This manuscript has associated data in a data repository. [Authors' comment: All data included in this manuscript are also available upon request by contacting with the corresponding author.]

Open Access This article is licensed under a Creative Commons Attribution 4.0 International License, which permits use, sharing, adaptation, distribution and reproduction in any medium or format, as long as you give appropriate credit to the original author(s) and the source, provide a link to the Creative Commons licence, and indicate if changes were made. The images or other third party material in this article are included in the article's Creative Commons licence, unless indi-

cated otherwise in a credit line to the material. If material is not included in the article's Creative Commons licence and your intended use is not permitted by statutory regulation or exceeds the permitted use, you will need to obtain permission directly from the copyright holder. To view a copy of this licence, visit <http://creativecommons.org/licenses/by/4.0/>.

References

1. G.R. Satchler, Phys. Rep. **199**, 147 (1991)
2. M.A. Nagarajan, C.C. Mahaux, G.R. Satchler, Phys. Rev. Lett. **54**, 1136 (1985)
3. M.E. Brandan, G.R. Satchler, Phys. Rep. **285**, 143 (1997)
4. C. Mahaux, H. Ngô, G.R. Satchler, Nucl. Phys. A **449**, 354 (1986)
5. L.F. Canto, P.R.S. Gomes, R. Donangelo, M.S. Hussein, Phys. Rep. **424**, 1 (2006)
6. M.S. Hussein, P.R.S. Gomes, J. Lubian, L.C. Chamon, Phys. Rev. C **73**, 044610 (2006)
7. P.R.S. Gomes, R.M. Anjos, C. Muri, J. Lubian, I. Padron, L.C. Chamon, R. Liguori Neto, N. Added, J.O. Fernández Niello, G.V. Martí et al., Phys. Rev. C **70**, 054605 (2004)
8. P.R.S. Gomes, M.D. Rodríguez, G.V. Martí, I. Padron, L.C. Chamon, J.O. Fernández Niello, O.A. Capurro, A.J. Pacheco, J.E. Testoni, A. Arazi et al., Phys. Rev. C **71**, 034608 (2005)
9. P.R.S. Gomes, I. Padrón, J.O. Fernández Niello, G.V. Martí, M.D. Rodríguez, O.A. Capurro, A.J. Pacheco, J.E. Testoni, A. Arazi, J. Lubian et al., Phys. G **31**, S1669 (2005)
10. S.B. Moraes, P.R.S. Gomes, J. Lubian, J.J.S. Alves, R.M. Anjos, M.M. Sant'Anna, I. Padrón, C. Muri, R. Liguori Neto, N. Added, Phys. Rev. C **61**, 064608 (2000)
11. M. Zadro, P. Figuera, A. Di Pietro, F. Amorini, M. Fisichella, O. Goryunov, M. Lattuada, C. Maiolino, A. Musumarra, V. Ostashko et al., Phys. Rev. C **80**, 064610 (2009)
12. A. Gómez Camacho, P.R.S. Gomes, J. Lubian, E.F. Aguilera, I. Padrón, Phys. Rev. C **76**, 044609 (2007)
13. P.R.S. Gomes, J. Lubian, B. Paes, V.N. Garcia, D.S. Monteiro, I. Padrón, J.M. Figueira, A. Arazi, O.A. Capurro, L. Fimiani et al., Nucl. Phys. A **828**, 233 (2009)
14. R.J. Woolliscroft, N.M. Clarke, B.R. Fulton, R.L. Cowin, M. Dasgupta, D.J. Hinde, C.R. Morton, A.C. Berriman, Phys. Rev. C **68**, 014611 (2003)
15. C. Signorini, A. Andrighetto, M. Ruan, J.Y. Guo, L. Stroe, F. Soramel, K.E.G. Löbner, L. Müller, D. Pierroutsakou, M. Romoli et al., Phys. Rev. C **61**, 061603(R) (2000)
16. N. Keeley, S.J. Bennett, N.M. Clark, B.R. Fulton, G. Tungate, P.V. Drumm, M.A. Nagarajan, J.S. Lilley, Nucl. Phys. A **571**, 326 (1994)
17. I. Martel, J. Gómez-Camacho, C. Blyth, N. Clarke, P. Dee, B. Fulton, J. Griffith, S. Hall, N. Keeley, G. Tungate, N. Davis, K. Rusek, K. Connell, J. Lilley, M. Bailey, Nucl. Phys. A **582**, 357 (1995)
18. I. Martel, J. Gómez-Camacho, K. Rusek, G. Tungate, Nucl. Phys. A **605**, 417 (1996)
19. A. Pakou, N. Alamanos, A. Lagoyannis, A. Gillibert, E.C. Pollacco, P.A. Assimakopoulos, G. Doukelisc, K.G. Ioannides, D. Karadimos, D. Karamanis et al., Phys. Lett. B **556**, 21 (2003)
20. A. Pakou, N. Alamanos, G. Doukelis, A. Gillibert, G. Kalyva, M. Kokkoris, S. Kossionides, A. Lagoyannis, A. Musumarra, C. Papachristodoulou et al., Phys. Rev. C **69**, 054602 (2004)
21. A. Pakou, N. Alamanos, N.M. Clarke, N.J. Davis, G. Doukelis, G. Kalyva, M. Kokkoris, A. Lagoyannis, T.J. Mertzimekis, A. Musumarra et al., Phys. Lett. B **633**, 691 (2006)
22. K. Zerva, A. Pakou, N. Patronis, P. Figuera, A. Musumarra, A. Di Pietro, M. Fisichella, T. Glodariu, M. La Commara, M. Lattuada, M. Mazzocco, M. Pellegriti, D. Pierroutsakou, A. Sanchez-Benitez, V. Scuderi, E. Strano, K. Rusek, Eur. Phys. J. A **48**, 102 (2012)

23. J.M. Figueira, J.O. Fernández Niello, D. Abriola, A. Arazi, O.A. Capurro, E. de Barbará, G.V. Martí, D. Martínez Heimann, A.E. Negri, A.J. Pacheco et al., *Phys. Rev. C* **75**, 017602 (2007)
24. J.O. Fernández-Niello, J.M. Figueira, D. Abriola, A. Arazi, O.A. Capurro, G.V. Martí, D. Martínez-Heimann, A.J. Pacheco, E. de Barbará, I. Padrón, P.R.S. Gomes, J. Lubian, *Nucl. Phys. A* **787**, 484c (2007)
25. J.M. Figueira, D. Abriola, J.O. Fernández Niello, A. Arazi, O.A. Capurro, E. de Barbará, G.V. Martí, D. Martínez Heimann, A.J. Pacheco, J.E. Testoni, I. Padrón, P.R.S. Gomes, J. Lubian, *Phys. Rev. C* **73**, 054603 (2006)
26. J.M. Figueira, J.O. Fernández Niello, A. Arazi, O.A. Capurro, P. Carnelli, L. Fimiani, G.V. Martí, D. Martínez Heimann, A.E. Negri, A.J. Pacheco et al., *Phys. Rev. C* **81**, 024613 (2010)
27. M. Biswas, S. Roy, M. Sinha, M.K. Pradhan, A. Mukherjee, P. Basu, H. Majumdar, K. Ramachandran, A. Shrivastava, *Nucl. Phys. A* **67**, 802 (2008)
28. A. Gómez Camacho, E.F. Aguilera, E. Martínez Quiroz, P.R.S. Gomes, J. Lubian, L.F. Canto, *Nucl. Phys. A* **833**, 156 (2010)
29. F.A. Souza, L.A.S. Leal, N. Carlin, M.G. Munhoz, R. Liguori Neto, M.M. de Moura, A.A.P. Suaide, E.M. Szanto, A. Szanto de Toledo, J. Takahashi, *Phys. Rev. C* **75**, 044601 (2007)
30. H. Kumawat, V. Jha, B.J. Roy, V.V. Parkar, S. Santra, V. Kumar, D. Dutta, P. Shukla, L.M. Pant, A.K. Mohanty, R.K. Choudhury, S. Kailas, *Phys. Rev. C* **78**, 044617 (2008)
31. A.M.M. Maciel, P.R.S. Gomes, J. Lubian, R.M. Anjos, R. Cabezas, G.M. Santos, C. Muri, S.B. Moraes, R.L. Neto, N. Added, N.C. Filho, C. Tenreiro, *Phys. Rev. C* **59**, 2103 (1999)
32. J. Lubian, I. Padron, P.R.S. Gomes, A.M.M. Maciel, R.M. Anjos, S.B. Moraes, J.J.S. Alves, C. Muri, R. Liguori Neto, N. Added, *Phys. Rev. C* **64**, 027601 (2001)
33. A. Sánchez-Benítez, D. Escrig, M.A.G. Álvarez, M.V. Andrés, C. Angulo, M.J.G. Borge, J. Cabrera, S. Cherubini, P. Demaret, J.M. Espino et al., *Nucl. Phys. A* **830**, 30 (2008)
34. L. Acosta, A.M. Sánchez-Benítez, M.E. Gómez, I. Martel, F. Pérez-Bernal, F. Pizarro, J. Rodríguez-Quintero, K. Rusek, M.A.G. Alvarez, M.V. Andrés et al., *Phys. Rev. C* **84**, 044604 (2011)
35. A.R. Garcia, J. Lubian, I. Padron, P.R.S. Gomes, T. Lacerda, V.N. Garcia, A. Gómez Camacho, E.F. Aguilera, *Phys. Rev. C* **76**, 067603 (2007)
36. E.F. Aguilera, E. Martinez-Quiroz, D. Lizcano, A. Gómez-Camacho, J.J. Kolata, L.O. Lamm, V. Guimarães, R. Lichtenthaler, O. Camargo, F.D. Becchetti et al., *Phys. Rev. C* **79**, 021601(R) (2009)
37. M. Mazzocco, N. Keeley, A. Boiano, C. Boiano, M. La Commara, C. Manea, C. Parascandolo, D. Pierrousakou, C. Signorini, E. Strano et al., *Phys. Rev. C* **100**, 024602 (2019)
38. A. Gómez Camacho, E.F. Aguilera, P.R.S. Gomes, J. Lubian, *Phys. Rev. C* **84**, 034615 (2011)
39. A. Gómez Camacho, E.F. Aguilera, *Phys. Rev. C* **90**, 064607 (2014)
40. V. Morcelle, R. Lichtenthaler, R. Linares, M.C. Morais, V. Guimarães, A. Lépine-Szily, P.R.S. Gomes, J. Lubian, D.R. Mendes Junior, P.N. De Faria et al., *Phys. Rev. C* **89**, 044611 (2014)
41. O. Sgouros, A. Pakou, D. Pierrousakou, M. Mazzocco, L. Acosta, X. Aslanoglou, C. Betsou, A. Boiano, C. Boiano, D. Carbone et al., *Phys. Rev. C* **94**, 044623 (2016)
42. O. Sgouros, A. Pakou, D. Pierrousakou, M. Mazzocco, L. Acosta, X. Aslanoglou, C. Betsou, A. Boiano, C. Boiano, D. Carbone et al., *Phys. Rev. C* **95**, 054609 (2017)
43. L. Fimiani, J.M. Figueira, G.V. Martí, J.E. Testoni, A.J. Pacheco, W.H.Z. Cárdenas, A. Arazi, O.A. Capurro, M.A. Cardona, P. Carnelli et al., *Phys. Rev. C* **86**, 044607 (2012)
44. N.N. Deshmukh, S. Mukherjee, D. Patel, N.L. Singh, P.K. Rath, B.K. Nayak, D.C. Biswas, S. Santra, E.T. Mirgule, L.S. Danu et al., *Phys. Rev. C* **83**, 024607 (2011)
45. S. Santra, S. Kailas, K. Ramachandran, V.V. Parkar, V. Jha, B.J. Roy, P. Shukla, *Phys. Rev. C* **83**, 034616 (2011)
46. S. Dubey, S. Mukherjee, D.C. Biswas, B.K. Nayak, D. Patel, G.K. Prajapati, Y.K. Gupta, B.N. Joshi, L.S. Danu, S. Mukhopadhyay et al., *Phys. Rev. C* **89**, 014610 (2014)
47. A. GómezCamacho, P.R.S. Gomes, J. Lubian, *Phys. Rev. C* **82**, 067601 (2010)
48. A. Mason, R. Chatterjee, L. Fortunato, A. Vitturi, *Eur. Phys. J. A* **39**, 107 (2009)
49. L. Fortunato, A. Vitturi, *Eur. Phys. J. A* **26**, 33 (2005)
50. I.J. Thompson, *FRESCO* (2007) **FRES**, 2.3 (2007)
51. C. Signorini, M. Mazzocco, G.F. Prete, F. Soramel, L. Stroe, A. Andrighetto, I.J. Thompson, A. Vitturi, A. Brondi, M. Cinausero et al., *Eur. Phys. J. A* **10**, 249 (2001)
52. C. Signorini, A. Edifizi, M. Mazzocco, M. Lunardon, D. Fabris, A. Vitturi, P. Scopel, F. Soramel, L. Stroe, G. Prete et al., *Phys. Rev. C* **67**, 044607 (2003)
53. M. Mazzocco, P. Scopel, C. Signorini, L. Fortunato, F. Soramel, I.J. Thompson, A. Vitturi, M. Barbui, A. Brondi, M. Cinausero et al., *Eur. Phys. J. A* **18**, 583 (2003)
54. M. Mazzocco, P. Scopel, C. Signorini, L. Fortunato, F. Soramel, I.J. Thompson, A. Vitturi, M. Barbui, A. Brondi, M. Cinausero et al., *Nucl. Phys. A* **746**, 497c (2004)
55. E. Fioretto, M. Cinausero, M. Giacchini, M. Lollo, G. Prete, R. Burch, M. Caldogno, D. Fabris, M. Lunardon, G. Nebbia, G. Viesti, A. Boiano, A. Brondi, G. La Rana, R. Moro, A. Ordine, E. Vardaci, A. Zagli, N. Gelli, F. Lucarelli, *IEEE Trans. Nucl. Sci.* **44**, 1017 (1997)
56. G. Prete, E. Fioretto, M. Cinausero, M. Giacchini, M. Lollo, D. Fabris, M. Lunardon, G. Nebbia, G. Viesti, M. Caldogno, A. Brondi, G. La Rana, R. Moro, E. Vardaci, A. Ordine, A. Zagli, A. Boiano, P. Blasi, N. Gelli, F. Lucarelli, *Il Nuovo Cimento A* **111**, 1089 (1998)
57. A. Ordine, A. Boiano, E. Vardaci, A. Zagli, A. Brondi, *IEEE Trans. Nucl. Sci.* **45**, 873 (1998)
58. M. Romoli, M. Di Pietro, E. Vardaci, A. De Francesco, M. Mazzocco, R. Bonetti, A. De Rosa, T. Glodariu, A. Guglielmetti, G. Inglima et al., *IEEE Trans. Nucl. Sci.* **52**, 1860 (2005)
59. M. Mazzocco, C. Signorini, M. Romoli, R. Bonetti, A. De Francesco, A. De Rosa, M. Di Pietro, L. Fortunato, T. Glodariu, A. Guglielmetti et al., *Eur. Phys. J. A Spec. Top.* **150**, 37 (2007)
60. D. Pierrousakou, B. Martin, T. Glodariu, M. Mazzocco, R. Bonetti, A. De Francesco, A. De Rosa, F. Farinon, A. Guglielmetti, G. Inglima et al., *Eur. Phys. J. Spec. Top.* **150**, 47 (2007)
61. C. Signorini, D. Pierrousakou, B. Martin, M. Mazzocco, T. Glodariu, R. Bonetti, A. Guglielmetti, M. La Commara, M. Romoli, M. Sandoli, E. Vardaci et al., *Eur. Phys. J. A* **63**, 44 (2010)
62. N. Patronis, A. Pakou, D. Pierrousakou, A.M. Sánchez-Benítez, L. Acosta, N. Alamanos, A. Boiano, G. Inglima, D. Filipescu, T. Glodariu et al., *Phys. Rev. C* **85**, 024609 (2012)
63. E.M. Kozulin, V.I. Zagrebaev, G.N. Knyazheva, I.M. Itkis, K.V. Novikov, M.G. Itkis, S.N. Dmitriev, I.M. Harca, A.E. Bondarchenko, A.V. Karpov, V.V. Saiko, E. Vardaci, *Phys. Rev. C* **96**, 064621 (2017)
64. A. Di Nitto, E. Vardaci, A. Brondi, G. La Rana, M. Cinausero, N. Gelli, R. Moro, P.N. Nadtochy, G. Prete, A. Vanzanella, *Phys. Rev. C* **93**, 044602 (2016)
65. R. Moro, A. Brondi, N. Gelli, M. Barbui, A. Boiano, M. Cinausero, A. Di Nitto, D. Fabris, E. Fioretto, G. La Rana, F. Lucarelli, M. Lunardon, G. Montagnoli, A. Ordine, G. Prete, V. Rizzi, M. Trotta, E. Vardaci, *Eur. Phys. J. A* **48**, 1 (2012)
66. A. Di Nitto, E. Vardaci, G. La Rana, P. Nadtochy, G. Prete, *Nucl. Phys. A* **971**, 21 (2018)
67. E. Vardaci, A. Di Nitto, P. Nadtochy, G. La Rana, *J. Phys. G: Nucl. Part. Phys.* **46**, 115111 (2019)
68. G. Igo, *Phys. Rev.* **115**, 1665 (1959)
69. N. Keeley, K. Rusek, *Phys. Rev. C* **56**, 3421 (1997)

70. S.Y. Lee, W. So, EPJ Web of Conference **17**, 16015 (2011)
71. J.J. Kolata, V.Z. Goldberg, L.O. Lamm, M.G. Marino, C.J. O’Keeffe, G. Rogachev, E.F. Aguilera, H. García-Martínez, E. Martínez-Quiroz, P. Rosales et al., Phys. Rev. C **65**, 054616 (2002)
72. V. Sargsyan, G.G. Adamian, N.V. Antonenko, P.R.S. Gomes, EPJ Web Conf. **69**, 00004 (2014)